



# Dynamic process of the massive Xinmo landslide, Sichuan (China), from joint seismic signal and morphodynamic analysis

Xiuqiang Bai<sup>1,2,3</sup> · Jihao Jian<sup>4</sup> · Siming He<sup>1,5,6</sup> · Wei Liu<sup>5,6</sup>

Received: 17 October 2017 / Accepted: 28 July 2018 / Published online: 13 August 2018  
© Springer-Verlag GmbH Germany, part of Springer Nature 2018

## Abstract

On 24 June 2017, a massive high-position landslide occurred at Diexi, Maoxian county, Sichuan, China, destroying the village of Xinmo with over 80 fatalities. Based on field surveys and DEM data before and after the landslide, the run-out of the landslide had a horizontal extent of 2400 m and a vertical extent of 1200 m and covered an area of about  $1.48 \times 10^6 \text{ m}^2$ . Based on the pre- and post-landslide profiles, the landslide region can be divided into four zones: source area, erosion area, sliding area, and accumulation area. The volume and area of each zone were calculated from DEM data before and after the landslide. Because of the fragmentation and erosion of the landslide during movement, the landslide volume increased from  $2.8 \times 10^6 \text{ m}^3$  to  $6.4 \times 10^6 \text{ m}^3$ ; the fractional amount of volume expansion due to fragmentation ( $F_F$ ) and entrainment ratio (ER) were 0.033 and 1.23, respectively. The velocity and acceleration of the Xinmo landslide were calculated through the inverted forces from seismic waves. The friction coefficients in each zone of the landslide during movement were also obtained, providing a useful parameter for numerical simulation modeling. An inverse relation was found between the absolute velocity and friction coefficient of each zone, demonstrating the existence of frictional velocity-weakening in massive extensive landslides. Based on frictional velocity-weakening, the steady-state apparent friction  $\mu(U, \sigma)$  as a function of absolute slip velocity  $U$  and normal pressure  $\sigma$  was also obtained.

**Keywords** Xinmo village landslide · Morphodynamic · Seismic signal · Frictional velocity-weakening

## Introduction

Landslides are serious secondary hazards, triggered by earthquakes or extreme precipitation events. Large-scale landslides cause significant damage, destroying homes and infrastructure,

cutting off pipelines and other utility lifelines, and blocking roads and stream drainages. Landslides have caused many deaths, injuries, and property loss (Jibson et al. 2004; Chigira 2009; Chigira et al. 2010; Chen et al. 2014b). Wen et al. (2004) defined massive landslides as having a minimum volume of  $10^7 \text{ m}^3$ . Massive landslides are always high-intensity and high-magnitude events. In most cases, intensity is used as a general term to describe landslide activity; intensity may refer to different parameters, such as volume, velocity, and size, while magnitude is used to describe the size of a landslide in terms of area or volume (Guzzetti 2000; Wen et al. 2004; Lateltin et al. 2005; Cigna et al. 2012; Meehan and Vahedifard 2013; Lari et al. 2014). To prevent or mitigate the risk of landslides, we should first focus on how to predict the processes of triggering, movement, and deposition of a landslide mass (Yang et al. 2014). In recent years, with the rapid development of computer and software technology, landslide researchers are increasingly utilizing numerical simulation to model the kinematics of massive high-velocity landslides with long run-out distances. For example, Wakai et al. (2015) used the dynamic elasto-plastic finite element method to simulate an earthquake-induced

✉ Siming He  
hsm@imde.ac.cn

<sup>1</sup> CAS Center for Excellence in Tibetan Plateau Earth Sciences, Beijing, China  
<sup>2</sup> Institute of Tibetan Plateau Research, Chinese Academy of Sciences, Beijing, China  
<sup>3</sup> University of Chinese Academy of Sciences, Beijing, China  
<sup>4</sup> College of Environment and Civil Engineering, Chengdu University of Technology, Chengdu, China  
<sup>5</sup> Key Laboratory of Mountain Hazards and Surface Process, Chinese Academy of Science, Chengdu, China  
<sup>6</sup> Institute of Mountain Hazards and Environment, Chinese Academy of Sciences, Chengdu, China

catastrophic landslide that occurred during the 2011 Great Tohoku and Kanto earthquake in Japan. The simulation showed a weakening of the apparent shear strength of sensitive materials during the long-distance movement of the landslide mass. Discontinuous deformation analysis (DDA) (Irie et al. 2009; Zhang et al. 2015), the material point method (MPM) (Numada et al. 2010; Llano-Serna et al. 2015), and the discrete element model (DEM) (Tang et al. 2012; Yuan et al. 2014) were also used to simulate the post-failure behavior of large-scale run-out processes during landslide movement. Numerical simulation was used to back-calculate landslide behavior (Wang et al. 2015; Beyabanaki et al. 2015; Zou et al. 2017; Gong and Tang 2017) and reveal its three stages of development: (i) pre-failure deformation, (ii) failure, and (iii) post-failure displacement or deformation. However, these approaches have some shortcomings. For example, some boundary conditions have to be assumed to obtain numerical solutions for the model to accurately simulate the behavior of the landslide. Moreover, the correct values of the material parameters (e.g., friction coefficient) are required for the numerical simulation models. At present, the material parameters are obtained mainly from laboratory tests; however, these values may not agree with the actual material parameters during massive landslide movement, leading to incorrect numerical simulation results.

To overcome these problems, seismic signals induced by landslide movement were inverted to determine the dynamic properties of landslides (Ekström and Stark 2013; Chen et al. 2014a; Lin 2015; Li et al. 2017; Hibert et al. 2017). The seismic signals generated by a high-speed massive landslide and recorded by seismic stations can be analyzed. Seismic wave signals can be divided into long-period waves and short-period waves. The low-frequency waves attenuate less; therefore, they travel farther than the high-frequency waves, and these signals can propagate more than 2000 km (Lin et al. 2010). While the short-period signals generated by a landslide attenuate rapidly away from the source, they have characteristic features, such as an emergent onset, no distinct phases, and no well-defined peak amplitude (Hibert et al. 2017). These characteristics are thought to be physically related to progressive failure of rock mass (McSaveney 2002), cracked rock impact during movement (Surinach et al. 2005; Deparis et al. 2008; Vilajosana et al. 2008), and mass bulking from erosion and scraping at the bottom of a landslide (Gauer and Issler 2004; Surinach et al. 2005). Thus, the key time points or duration of the landslide may be inferred from the features of the seismic signals to identify the landslide initiation and sliding sequence.

From the perspective of the whole region, the spatial range of Xinmo village landslide is small compared with the wavelength of the seismic signals and the distance between the event and the seismic stations; therefore, the force induced by the Xinmo village landslide acting on the crust of the earth

during movement can be treated as a time-varying point force, which can be obtained through a source inversion with the long-period seismic records. While from a single landslide scale, the force also depended on the terrain which the landslide slid on. In other words, the force added space attributes, which needed to be considered under certain circumstances. In addition, the pre- and post-digital elevation model (DEM) data could be used to supply the profiles of landslides before and after sliding and calculate the run-out distance and the area and volume of the landslide zone. In this paper, pre- and post-DEM and seismic signal data are combined to analyze the dynamic properties of the Xinmo landslide, which destroyed the village of Xinmo in Sichuan province, China, on 24 June 2017.

## The Xinmo landslide

At 5:39 on 24 June 2017, a massive high-position landslide-debris avalanche occurred on Fugui Mountain at Xinmo village (103°39'03.4"E, 32°04'09.4"N) in Diexi town, Maoxian County, Sichuan Province, China, causing great loss of life and property. Ten deaths were reported and 73 missing as well as 46 houses buried under the landslide. At the top of the mountain, a cracked rock mass suddenly ruptured along its fracture surface and began to slide downward, entraining surface sediment and then transforming into a granular flow. Finally, the landslide destroyed the village of Xinmo and blocked the Songpinggou River, forming a dammed lake 2 km long and burying a 2.1 km section of the road (Township Road No. 104). Based on seismic signals recorded by Sichuan seismic stations, the landslide lasted about 120 s. According to the field investigation and remote sensing interpretation, the run-out of the landslide extended 2400 m horizontally and 1200 m vertically, which is equivalent to an effective friction angle of 27° (the angle of the line connecting the head of the landslide source to the distal boundary of the displaced mass) and covered an area about  $1.48 \times 10^6 \text{ m}^2$ . To the west of the source, erosion and accumulation areas of the landslide, deformation areas were observed (Fig. 1), which may have been caused by the strain produced by the landslide during its movement.

## Geologic conditions and topography

Xinmo village is located on Mt. Fugui in the middle section of the Longmen mountain fault zone, where folds and fault structures are very developed. The Triassic Zagunao group is exposed above the landslide site, with light gray thin and medium-thick layered metamorphic quartz sandstone, oriented  $280^\circ \angle 53^\circ$ ; these strike and dip directions are close to the main slip direction, which is SW. There are two dominant

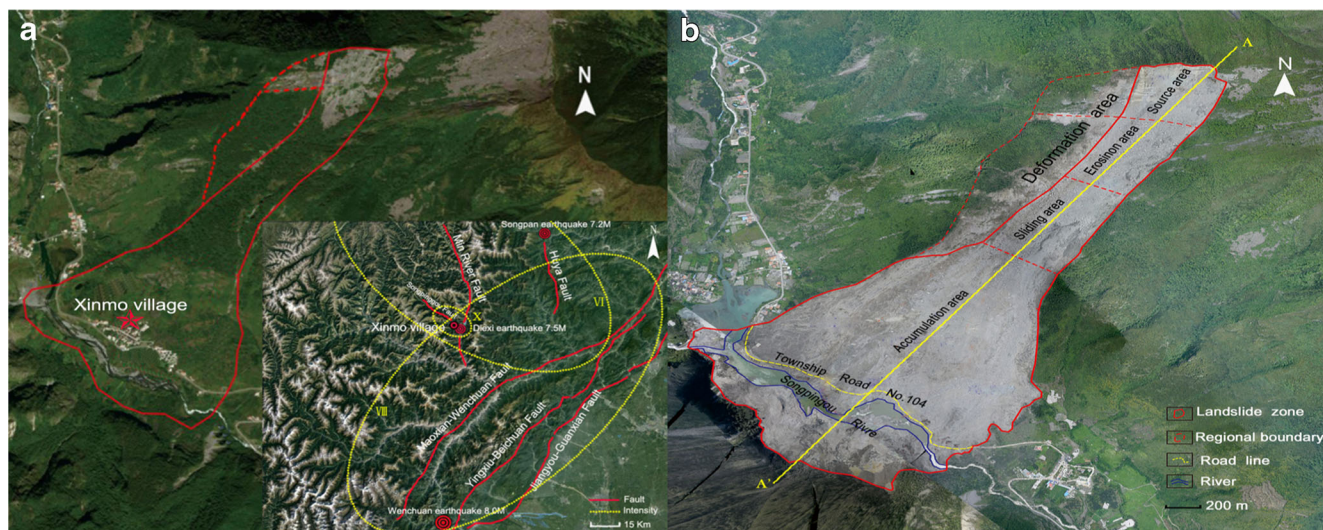


**Fig. 1** 3D images showing catastrophic landslide at Xinmo village (red star), Diexi town, Sichuan province, China **a** The site before the event, inserts: faults and intensity of historic earthquakes ( $\geq 7.2$  M) around the Xinmo village **b** the landslide after the event

structural planes:  $100^{\circ}\angle 70^{\circ}$  and  $350^{\circ}\angle 40^{\circ}$ . Notably, the area is located in the epicenter area of the 7.5 M Diexi earthquake, which occurred in 1933. The area was also affected by the 8.0 M Wenchuan earthquake in 2008; therefore, the rock joints and fissures in the area are well developed.

According to the field investigation and pre-DEM interpretation, this section of the Songpinggou River runs in a V-shaped canyon, with an elevation difference of over 1600 m. The slopes on both sides of the mountain are steep, the elevation difference of the left bank slope is 1250 m, and the dip of the middle and upper parts of the slope is greater than  $50^{\circ}$ , which provides natural conditions for the occurrence of landslides.

## Seismic history

Faults are widely developed in the study area; the major faults in the area are the Maoxian-Wenchuan fault, Yingxiu-Beichuan fault, Jiangyou-Guanxian fault, Minjiang fault, and Songpinggou fault (Fig. 1). The region experienced many earthquakes; data of the China seismic network shows that Xinmo village was most influenced by the Diexi earthquake, Songpan earthquake, and Wenchuan earthquake. These events produced many cracks in the area. The epicenter of the Diexi earthquake is only 3.97 km from Xinmo village (Chai and Liu 1995); therefore, Xinmo was seriously affected by this earthquake, which reached X on the Chinese seismic intensity scale. The study site experienced an intensity of VI during the 1976 Songpan earthquake and an intensity of VIII during the 2008 Wenchuan earthquake (Chen et al. 1994; Dong et al. 2008).

## Climate and rainfall characteristics

The study area is in the temperate climatic zone, with a dry climate and low temperatures. It is generally dry and windy, cold in the winter, and cool in the summer. With complex topography, the vertical climate differences are prominent with large differences in temperature between the valley and mountain top. Additionally, a large temperature difference exists between day and night, which accelerates the freeze-thaw cycles of rocks and gradually changes the properties of the slope body. The town's annual average temperature and annual rainfall is about  $13.5^{\circ}\text{C}$  and 800 mm, respectively. The rainfall distribution throughout the year is uneven and occurs mainly during May–Oct. The average temperature is  $5^{\circ}\text{C}$  in January and  $22.5^{\circ}\text{C}$  in July.

During the 2017 rainy season, the rainfall in Maoxian was much higher than in previous years, especially during 1–23 June when 42% more rainfall was recorded than during the corresponding period in 2015–16. According to the two precipitation observation sites near Diexi and Songpinggou, the total rainfall from June 8 to 14 was more than 200 mm (Fig. 2). The infiltration of the precipitation along the cracks in the rock fissure led to the rapid decrease of the sliding resistance of the landslide mass, which triggered the landslide.

## Post-failure behavior of the Xinmo landslide

The DEM is a digital model that represents the elevation of the ground in a set of ordered numerical arrays. The DEM data of the study site before the landslide were provided by the Sichuan Geomatics Center with a precision of 5 m. One day after the accident, the Sichuan Geomatics Center performed



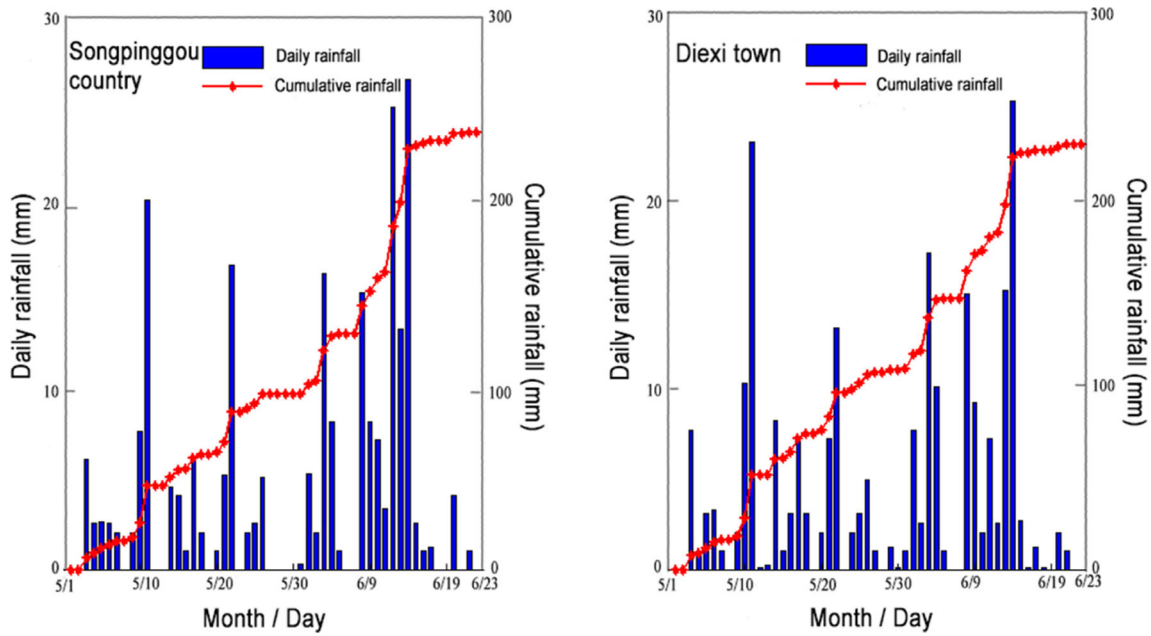


Fig. 2 Daily rainfall and cumulative rainfall from 1st May to 23rd June at two rainfall observation stations near Xinmo village

aerial photogrammetry with high-performance UAV to obtain high-resolution elevation with 0.5 m precision. Figure 3a shows the ground elevation along profile AA' (shown in Fig. 1) before and after the Xinmo landslide. Based on the pre- and post-landslide profiles, the landslide region can be divided into four zones: source area, erosion area, sliding area, and accumulation area (Fig. 3a). Each volume of the landslide region can be determined by the difference in elevation before and after the sliding event, which was obtained from the pre- and post-landslide DEM data in a geographic information systems (GIS). As the sliding area was less affected by erosion,

the area and volume of the erosion and high-speed areas were calculated together. The area and volume of the landslide zones were shown in Table 1. The thickness of the landslide accumulation is shown in Fig. 3b.

Based on the volume of each zone of the Xinmo landslide, the fractional amount of volume expansion due to fragmentation ( $F_F$ ) and the entrainment ratio ( $ER$ ) were obtained based on Hungr and Evans (2004). The equations can be expressed as:

$$V = V_E + V_R(1 + F_F) \tag{1}$$

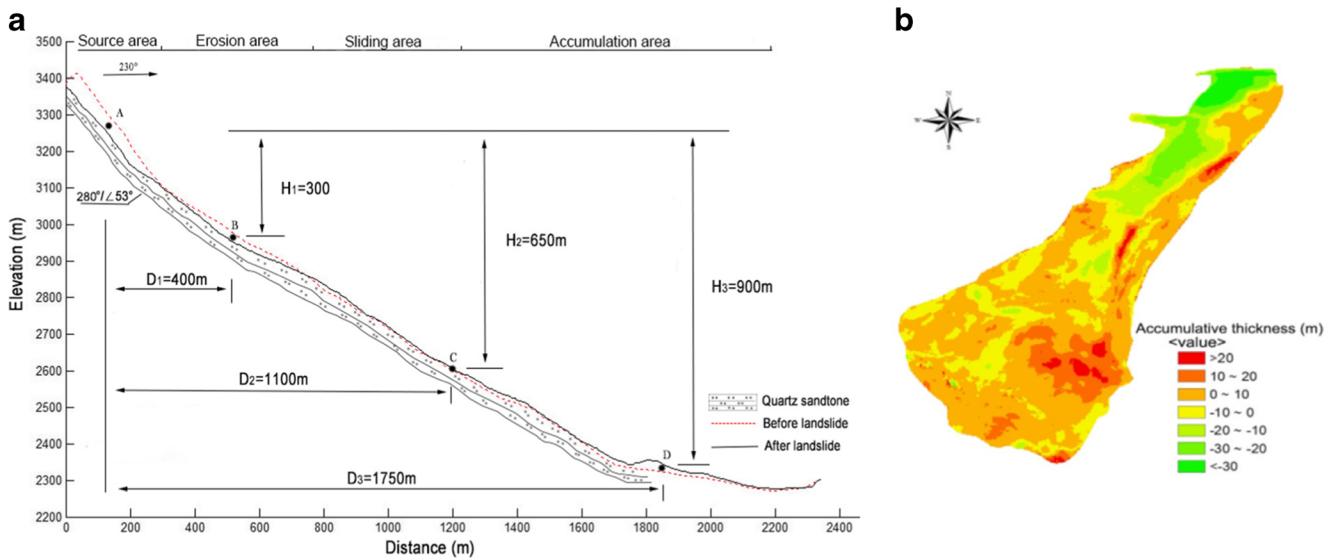


Fig. 3 a Profile AA' (shown in Fig. 1) showing the ground surface before the Xinmo landslide (red dashed line) and after the landslide (solid black line), derived from pre- and post-event DEMs. A, B, and D represent the

centroids of source area, erosion area, and accumulation area, respectively b Landslide accumulation thickness

**Table 1** The area and volume of each zone of the Xinmo village landslide

Landslide zonings	Area (m <sup>2</sup> )	Volume (m <sup>3</sup> )
Source area	90,450	-2,838,241.29
Erosion and sliding areas	562,725	-3,494,357.056
Accumulation area	836,675	6,426,911.2

$$ER = \frac{V_{Entrained}}{V_{Fragmented}} = \frac{V_E}{V_R(1 + F_F)} \tag{2}$$

where  $V$  is the accumulated landslide volume,  $V_E$  is the volume of the entrained material, and  $V_R$  is the volume of the source area. Using Eqs. (1) and (2), we obtained  $F_F=0.033$  and  $ER=1.23$ .

To analyze the dynamic properties of the Xinmo landslide we used seismic data collected by seismic stations near the Xinmo village in Sichuan province (Fig. 4a). From the waveforms recorded by seismic stations around the Xinmo village (Fig. 4b), the Xinmo village landslide movement process can be easily identified from the waveforms. The MXI station waveform showed a significant change in a small section (about 20s long) of the seismic time series at approximately 5:30 am on 24 June 2017, about 9 min before the landslide occurred (Fig. 5a). This prominent signal may have been generated by elastic rebound of the shallow crust induced by the fracture of a critical segment in the cracked rock (Lin et al. 2010). For the study, the data from the seismic stations around the Xinmo village were used to invert the source time functions (Fig. 4b). In order to invert the source time functions, the seismic data were processed

in the following procedure: first, the means were removed from each time series and corrected for the instrumental response in all waveforms; second, the time series of the seismic data were transformed to the frequency domain using the fast Fourier transform (FFT) to reveal the spectral contents of the signals and then the seismic signals were passed through a Butterworth band-pass filter based on the spectral contents of the signals (Fig. 5b); third, the records were then integrated once in the time domain to obtain displacements; fourth, the source time functions could be deconvolved from the displacements with Green’s functions, which have been well developed in recent decades (Nakano et al. 2008; Yamada et al. 2013; Allstadt 2013; Li et al. 2017). In this paper, we mainly used the methods in Li et al. (2017) and Wang (1999) to obtain Green’s functions and the source time functions (Fig. 6).

Because the fragmentation ( $F_F$ ) ratio of Xinmo landslide is only 0.033, we could treat the landslide as a rigid block sliding along a well-defined slip surface, which is similar to the Newmark method (Newmark 1965; Ingles et al. 2006; Jibson 2007); while the difference between them is the acceleration of the Xinmo village landslide obtained by dividing the inertial force by the mass not by an earthquake acceleration exceeding the critical acceleration. In order to analyze the dynamic process of the massive Xinmo landslide, the velocity of the landslide is the integral of the acceleration over time (i.e.,  $v=\int dt/m$ ), and the displacement is the double-integral of the acceleration over time.

In previous studies of dynamic landslide processes revealed by broadband seismic records (Yamada et al. 2013; Ekström and Stark 2013; Li et al. 2017), the mass of the landslide was assumed a constant throughout the movement

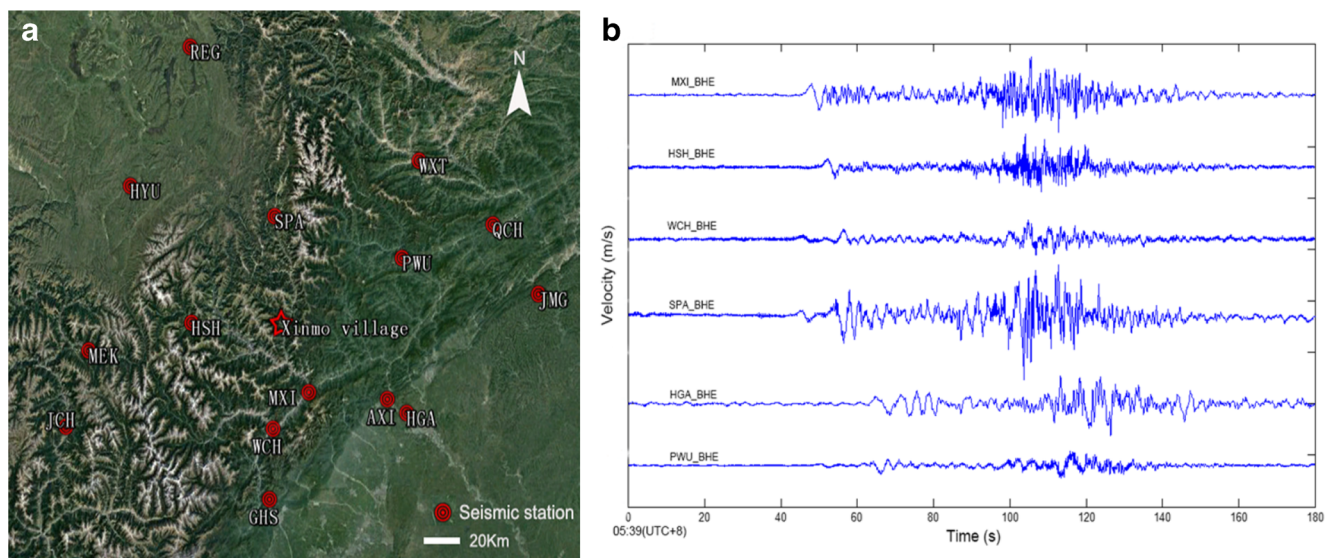


**Fig. 4** a Location of seismic stations around Xinmo village b Seismic signals (EW component of horizontal acceleration) recorded by near seismic stations

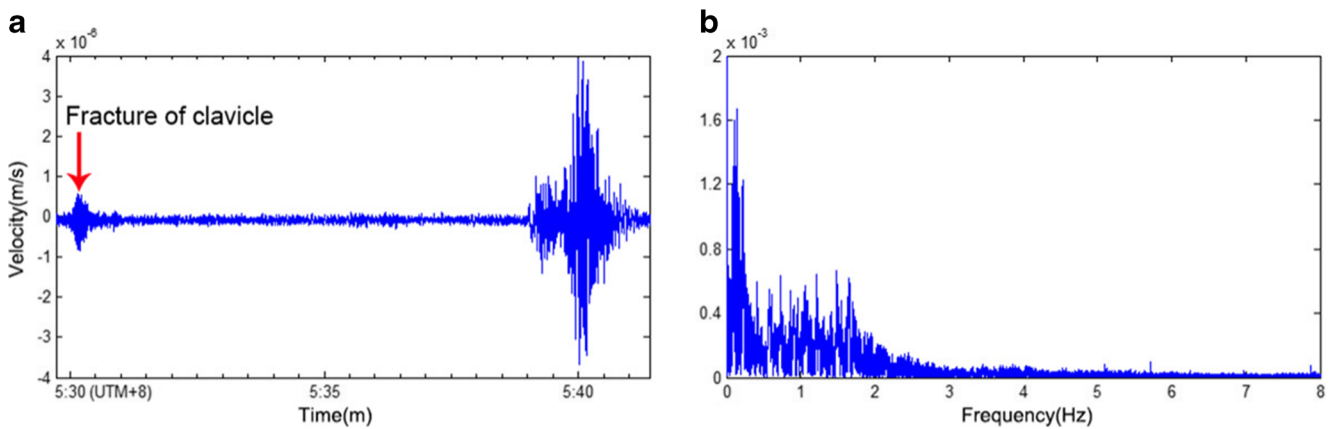


**Fig. 5** Seismograms recorded at station MXI; (a) time series from 5:30 am to 5:42 am (b) frequency spectrum obtained from the time series through the fast Fourier transform (FFT)

without considering erosion. While according to Fig. 3a, it is obvious that the source area and the erosion area exist on the profile AA'. That means if the mass of the Xinmo village landslide was represented by the total mass of the landslide at the beginning, especially if there is an obvious erosion area, it may not reflect the real state of movement. In addition, the mass of source area and erosion area could be calculated through Table 1, assuming a density of  $2.5 \times 10^3 \text{ kg/m}^3$ , and the total mass of the landslide could be calculated by adding

the mass of source area and erosion area. In order to study the effect of the mass of the landslide represented by the total mass or only by the mass of the source material at the beginning of the landslide movement process, in this paper, two scenarios will be considered: in the first scenario, the mass of the landslide was considered as a constant during movement, namely, the mass of the landslide is the total mass in the entire movement; in the second scenario, the mass of the landslide was only the mass of the source area until the landslide

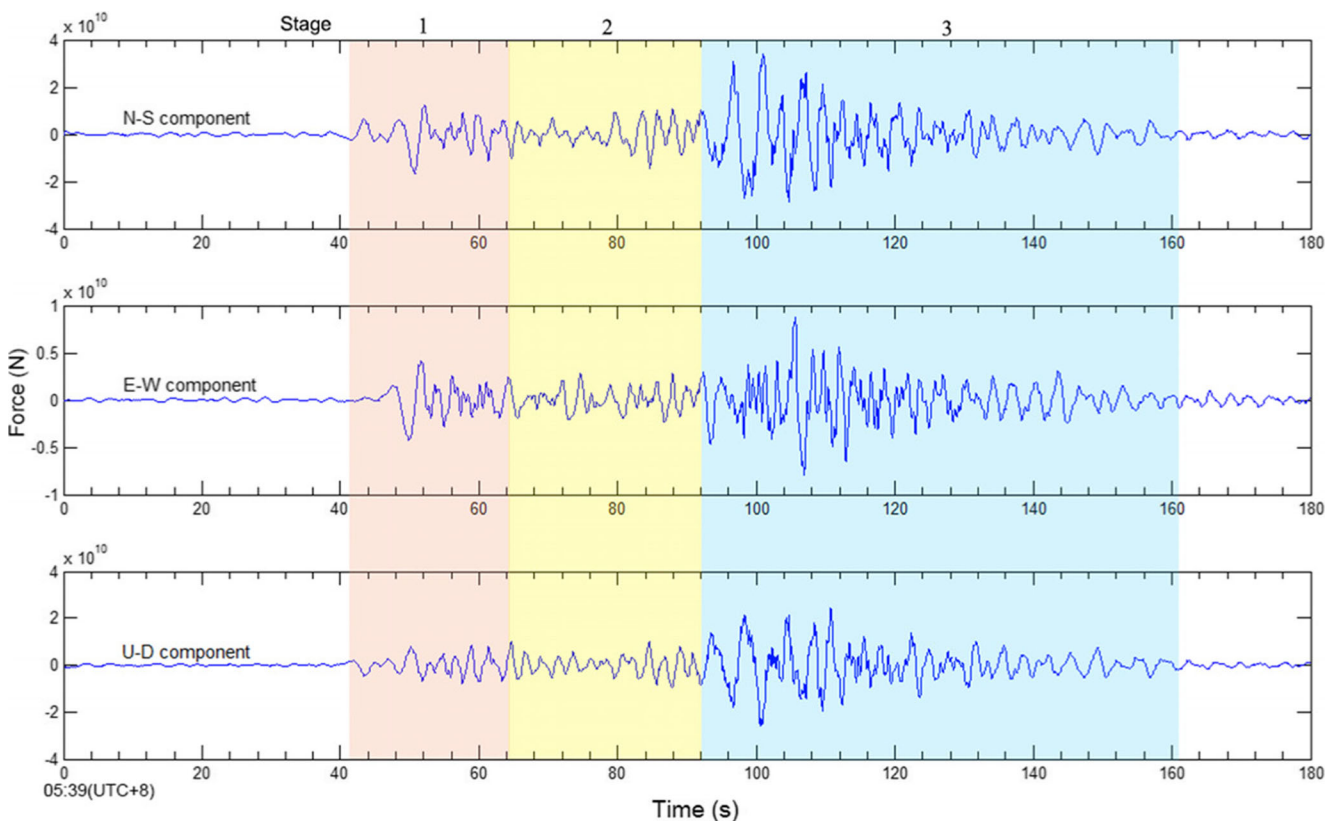


**Fig. 6** Estimated single-force source time functions of the Xinmo village landslide inverted by seismic stations around the Xinmo village. Different colors represent three different stages of the landslide movement, labeled 1–3

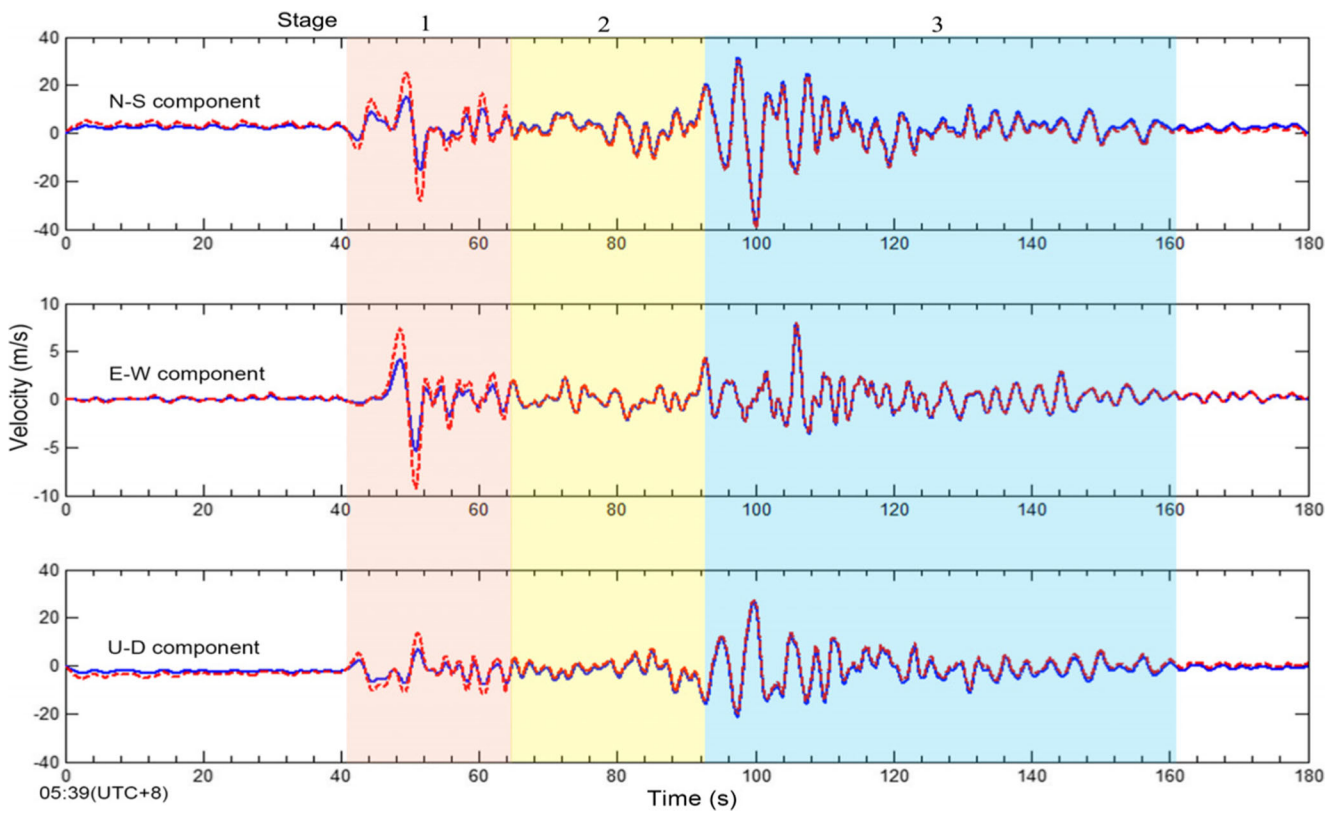


**Fig. 7** Estimated velocity of the N-S component, E-W component, and U-D component in the first scenario (blue line) and the second scenario (red dash line). Different colors represent three different stages of the landslide movement, labeled 1–3

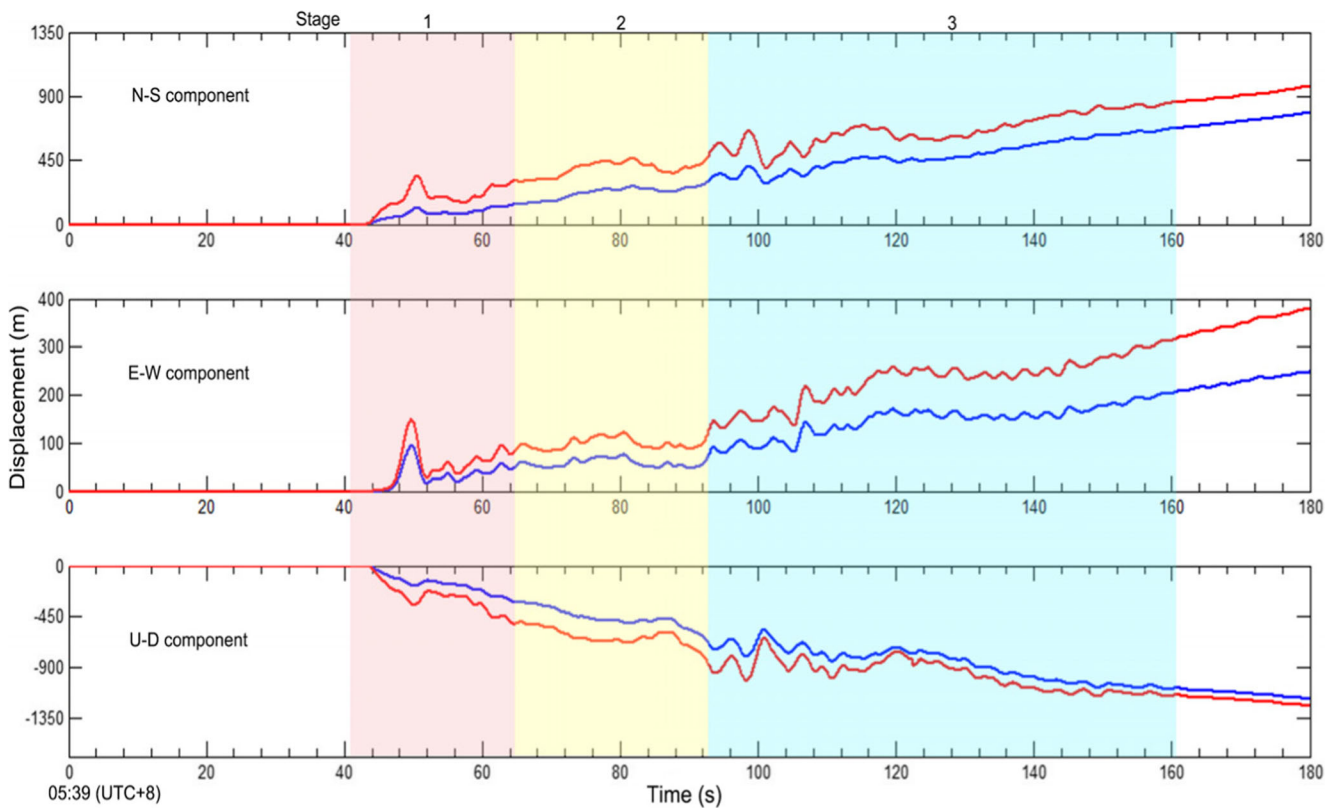


**Fig. 8** Estimated displacement of the N-S component, E-W component, and U-D component in the first scenario (blue) and the second scenario (red). Different colors represent three different stages of the landslide movement, labeled 1–3



arrived at the erosion area and became the total mass of the landslide. We take the erosion into consideration in the second scenario, which aims to reveal the differences between the two scenarios above.

In the first scenario, owing to the mass of the landslide being considered as a constant, the acceleration of the landslide could be obtained by dividing the inertial force by the total mass, the velocity is the integral of the acceleration over time, and the displacement is the integral of the velocity over time. While the second scenario differs from the first scenario because the mass of the landslide was only the mass of the source area before colliding with the erosion zone, and the source zone and the erosion zone were treated as rigid blocks along the slip surface for simplicity. When they collided, the collision process was considered as conservation of momentum. A detailed analysis of the dynamic process of the Xinmo landslide is as follows:

- 1) In the first stage (41–64 s): the landslide occurred and moved from the source area to erosion area. Because the mass of the landslide was smaller in the second scenario than the first scenario, the velocity of the landslide in the second scenario is larger than that in the first scenario (Fig. 7), which also induced the displacement difference in the same time (Fig. 8). Comparing the displacement with the profile AA' shows that the second scenario is more reasonable. After 48 s, the estimated source functions and velocity in the E-W component started to decrease to zero and then reverse, reaching peak values in the opposite direction at around 51 s, indicating deceleration of the landslide in the E-W component and collision with the west side slope, according to field investigation. Approaching 64 s, the rigid block of the source zone impacted with the erosion zone and became as a whole, this process followed the conservation of momentum; since, even if they were the same speed, their displacements were different in latter stages.
- 2) In the second stage (64–92 s): according to Figs. 3a and 6, the terrain in this section (sliding area) is relatively smooth and narrow, which induced the estimated source functions and velocity of sliding mass to be relatively stable.
- 3) In the third stage (92–161 s): after 92 s, the sliding mass reached the old landslide deposits and constantly accumulated energy, which induced the estimated source functions and the velocity of the sliding mass to begin to increase and reach peak values in the whole process. Owing to the open terrain, the sliding mass was further fragmented without confining pressure and decelerated slowly to zero. Approaching 98 s, according to Figs. 6 and 8, the sliding mass rebounded in the N-S component and the U-D component, which may have been induced by impacting with the Xinmo village.

## Discussion and conclusions

Combining DEM data with seismic wave signals of the Xinmo landslide, the areas and volumes of each zone of the landslide and the values of the dynamic parameters of the landslide were calculated. The sliding mass was treated as an ideal sliding rigid block, and the basal friction coefficient could be calculated by the following equation:

$$mg(\sin\theta - \mu\cos\theta) = f \quad (3)$$

where  $m$  is the mass,  $g$  is the angle of the slope,  $\theta$  is the angle of the slope,  $\mu$  is the basal friction coefficient, and  $f$  is the inertial force of the sliding mass along the slope.  $\mu$  is the only unknown variable in Eq. (3). Figure 9 shows an inverse relation between the absolute velocity and friction coefficient of each stage. The results indicated that frictional velocity-weakening occurs in massive long run-out landslides, in agreement with the findings of Lucas et al. (2014), Yang et al. (2014), and Dong et al. (2013, 2014). According to Eq. (3), the change of friction coefficient was mainly caused by the change of velocity induced by the inertial force of the sliding mass along the slope. While some studies show that the normal stress of the sliding block affects the friction (Guo 2004; Yang et al. 2015; Wang et al. 2018). There is an inverse power law relationship between the friction and its corresponding normal stress. Based on the previous academic research (Guo 2004; Dong et al. 2013; Lucas et al. 2014; Yang et al. 2014; Yang et al. 2015; Wang et al. 2018), we propose the steady-state apparent friction as a function of absolute slip velocity  $U$  and normal pressure  $\sigma$ :

$$\mu(U, \sigma) = \mu_{\infty} + (\mu_0 - \mu_{\infty})e^{-\left(\frac{U}{U_w} + \frac{\sigma}{\sigma_0}\right)} \quad (4)$$

where  $\mu(U, \sigma)$  represents the steady-state apparent friction of the landslide at an absolute slip velocity  $U$  and a normal stress  $\sigma$ ,  $\mu_0$  is the static apparent frictions of the material, and  $\mu_{\infty}$  is the the steady-state friction coefficient when the slip velocity or normal pressure approach infinity.  $U_w$  is the material constant and  $\sigma_0$  is an equal order of magnitude of  $\sigma$  to keep coincidence with Yang et al. (2015) (Fig. 10). In this paper, the value of  $\mu_{\infty}$  is 0.2 taken from previous studies, and the normal stress  $\sigma$  can be calculated by the inertial force. As a result, Fig. 10 is found similar to the figure of the steady-state apparent friction  $\mu(U)$  or  $\mu(\sigma)$  in the previous academic research.

Comparing the first scenario with the second scenario we can learn that if there was an obvious erosion area, we should take the second scenario into consideration, otherwise there will be great difference with the actual state. We also should note that we treated the source as a time-varying point, the velocity and the displacement are only for the center of the sliding mass, and do not cover the total range of the landslide.



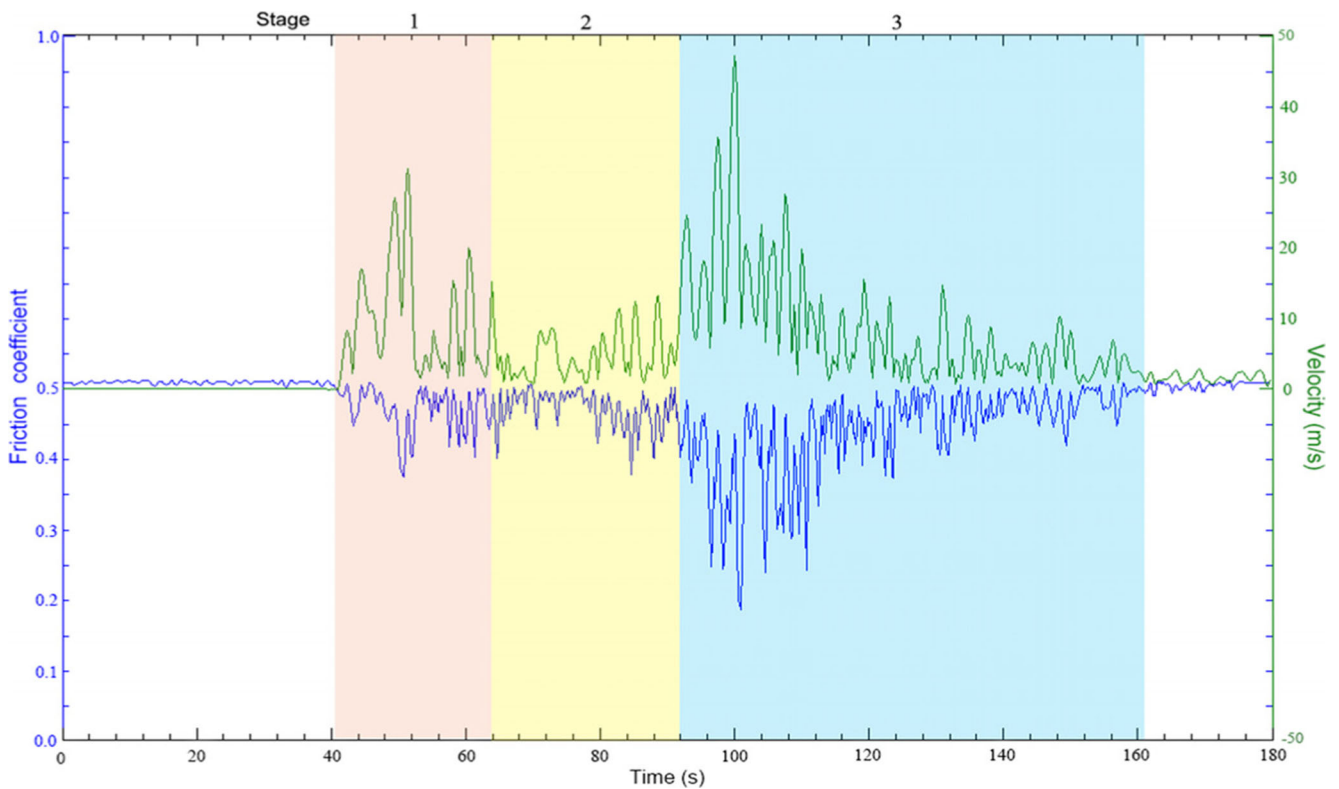


**Fig. 9** The absolute velocity of the sliding body (green line) and the basal friction coefficients (blue line). Different colors represent three different stages of the landslide movement, labeled 1–3

Based on the above analysis, the following conclusions were drawn. (1) The large-scale landslide that destroyed the village of Xinmo was triggered by continual rainfall in an area containing extensive faults and cracks induced by historical earthquakes. This indicates that earthquake damage to soil or

rock mass can make the affected area prone to geological hazards for decades. (2) Combining DEM of the landslide area with seismic wave signals, the motion of the Xinmo landslide was reproduced. (3) The analysis was also used to derive the friction coefficient, which can be used in numerical simulation

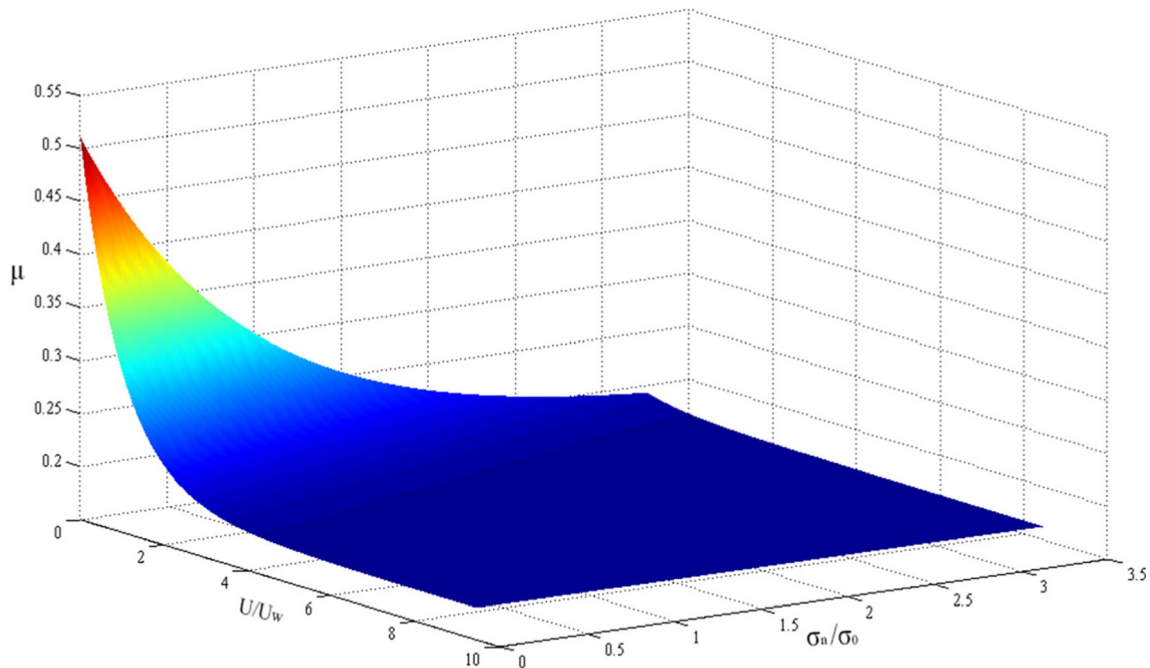


**Fig. 10** The steady-state apparent friction of the landslide  $\mu(U, \sigma)$  at an absolute slip velocity  $U$  and a normal stress  $\sigma$

models to improve the results of landslide simulations. (4) Comparing the pre- and post-DEM data, the thickness of the accumulation zone was obtained; this important information can be helpful for emergency response crews at the scene during rescue operations. (5) Although the pre-landslide DEM data has only a precision of 5 m, and there will be errors in estimating the volume of landslide that may affect the estimation of the velocity and mass of the landslide, the mass of the landslide can be calibrated by the sliding distance of the field survey and the movement time inferred from seismic waves. This method is also useful to analyze the dynamic properties of the Xinmo landslide and reveal frictional velocity-weakening occurring in massive long run-out landslides.

**Acknowledgments** This work was supported as a joint research project by NSFC-ICIMOD (Grant No. 41661144041); the NSFC (Grant No. 41772312); The Key Research and Development Program and The Scientific Support Program of the Science and Technology Department of Sichuan Province of China (Grant No.2017SZ0041; Grant No.2016SZ0067). We are thankful for the DEMs data of the study site provided by Sichuan Geomatics Center and the seismic data and suggestions provided by the Sichuan Earthquake Administration. We also thank the previous reviewers and Dr. A. Lucas for helpful suggestions, which greatly improved the quality of this paper.

## References

- Allstadt K (2013) Extracting source characteristics and dynamics of the August 2010 Mount Meager landslide from broadband seismograms. *J Geophys Res Earth Surf* 118(3):1472–1490
- Beyabanaki SAR, Bagtzoglou AC, Liu L (2015) Applying disk-based discontinuous deformation analysis (DDA) to simulate Donghekou landslide triggered by the Wenchuan earthquake. *Geomech Geoeng* 11(3):177–188
- Chai H, Liu H (1995) Landslide dams induced by diexi earthquake in 1933 and its environmental effect. *J Geol Hazard Environ Preserv* 6(1):7–17 (in Chinese)
- Chen SF et al (1994) Active faulting and block movement associated with large earthquakes in the Min Shan and Longmen Mountains, north-eastern Tibetan Plateau. *J Geophys Res Solid Earth* 99(B12):24025–24038
- Chen TC, Lin ML, Wang KL (2014a) Landslide seismic signal recognition and mobility for an earthquake-induced rockslide in Tsaoiling, Taiwan. *Eng Geol* 171:31–44
- Chen Q, Cheng H, Yang Y, Liu G, Liu L (2014b) Quantification of mass wasting volume associated with the giant landslide Daguangbao induced by the 2008 Wenchuan earthquake from persistent scatterer InSAR. *Remote Sens Environ* 152:125–135
- Chigira M (2009) September 2005 rain-induced catastrophic rockslides on slopes affected by deep-seated gravitational deformations, Kyushu, southern Japan. *Eng Geol* 108(1–2):1–15
- Chigira M et al (2010) Landslides induced by the 2008 Wenchuan earthquake, Sichuan, China. *Geomorphology* 118(3–4):225–238
- Cigna F, Bianchini S, Casagli N (2012) How to assess landslide activity and intensity with Persistent Scatterer Interferometry (PSI): the PSI-based matrix approach. *Landslides* 10(3):267–283
- Deperis J et al (2008) Analysis of Rock-Fall and Rock-Fall Avalanche Seismograms in the French Alps. *Bull Seismol Soc Am* 98(4):1781–1796
- Dong JJ, Yang CM, Yu WL, Lee CT, Miyamoto Y, Shimamoto T (2013) Velocity-displacement dependent friction coefficient and the kinematics of giant landslide. *Earthquake-Induced Landslides*. Springer, Berlin. [https://doi.org/10.1007/978-3-642-32238-9\\_41](https://doi.org/10.1007/978-3-642-32238-9_41)
- Dong JJ, Tsao CC, Yang CM, Wu WJ, Lee CT, Lin M L et al (2014) The geometric characteristics and initiation mechanisms of the earthquake-triggered Daguangbao landslide. In: Hazarika H, Kazama M, Lee W (eds) *Geotechnical hazards from large earthquakes and heavy rain-falls*. Springer, Tokyo. [https://doi.org/10.1007/978-4-431-56205-4\\_19](https://doi.org/10.1007/978-4-431-56205-4_19)
- Dong S, Zhang Y, Wu Z, Yang N, Ma Y, Shi W et al (2008) Surface rupture and co-seismic displacement produced by the Ms 8.0 Wenchuan earthquake of May 12, 2008, Sichuan, China: eastwards growth of the Qinghai-Tibet plateau. *Acta Geol Sin* 82(5):938–948 (in Chinese)
- Ekström G, Stark C.(2013) Simple scaling of catastrophic landslide dynamics. *Science* 339(6126):1416–1419. <http://www.jstor.org/stable/41942420>
- Gauer P, Dieter I (2004) Possible erosion mechanisms in snow avalanches. *Ann Glaciol* 38:384–392
- Gong B, Tang C (2017) Slope-slide simulation with discontinuous deformation and displacement analysis. *International Journal of Geomechanics* 17(5):E4016017
- Guo Y (2004) Influence of normal stress and grain shape on granular friction: results of discrete element simulations. *J Geophys Res* 109(B12). <https://doi.org/10.1029/2004JB003044>
- Guzzetti F (2000) Landslide fatalities and the evaluation of landslide risk in Italy. *Eng Geol* 58:89–107
- Hibert C, Ekström G, Stark CP (2017) The relationship between bulk-mass momentum and short-period seismic radiation in catastrophic landslides. *J Geophys Res Earth Surf* 122(5):1201–1215
- Hungr O, Evans SG (2004) Entrainment of debris in rock avalanches: an analysis of a long run-out mechanism. *Geol Soc Am Bull* 116(9):1240
- Ingles J et al (2006) Effects of the vertical component of ground shaking on earthquake-induced landslide displacements using generalized Newmark analysis. *Eng Geol* 86(2–3):134–147
- Irie K, Koyama T, Hamasaki E et al. (2009) DDA simulations for huge landslides in Aratozawa area, Miyagi, Japan caused by Iwate-Miyagi Nairiku earthquake. <https://doi.org/10.3850/9789810844554-0057>
- Jibson RW (2007) Regression models for estimating coseismic landslide displacement. *Eng Geol* 91(2–4):209–218
- Jibson RW et al (2004) Landslides Triggered by the 2002 Denali Fault, Alaska, earthquake and the inferred nature of the strong shaking. *Earthquake Spectra* 20(3):669–691
- Lari S, Frattini P, Crosta GB (2014) A probabilistic approach for landslide hazard analysis. *Eng Geol* 182:3–14
- Lateltin O et al (2005) Landslide risk management in Switzerland. *Landslides* 2(4):313–320
- Li Z, Huang X, Xu Q, Yu D, Fan J, Qiao X (2017) Dynamics of the Wulong landslide revealed by broadband seismic records. *Earth Planets Space* 69(1):27
- Lin C-H (2015) Insight into landslide kinematics from a broadband seismic network. *Earth Planets Space* 67(1):8
- Lin CH, Kumagai H, Ando M, Shin TC (2010) Detection of landslides and submarine slumps using broadband seismic networks. *Geophys Res Lett* 37(22):333–345. <https://doi.org/10.1029/2010GL044685>
- Llano-Serna MA, Farias MM, Pedroso DM (2015) An assessment of the material point method for modelling large scale run-out processes in landslides. *Landslides* 13(5):1057–1066
- Lucas A, Mangeney A, Ampuero JP (2014) Frictional velocity-weakening in landslides on Earth and on other planetary bodies. *Nat Commun* 5:3417
- McSaveney MJ (2002) Recent rockfalls and rock avalanches in Mount Cook National Park, New Zealand. *Geol Soc Am Rev Eng Geol* XV:35–70. <https://doi.org/10.1130/REG15-p35>
- Meehan CL, Vahedifard F (2013) Evaluation of simplified methods for predicting earthquake-induced slope displacements in earth dams and embankments. *Eng Geol* 152(1):180–193

- Nakano M et al (2008) Waveform inversion in the frequency domain for the simultaneous determination of earthquake source mechanism and moment function. *Geophys J Int* 173(3):1000–1011
- Newmark NM (1965) Effects of earthquakes on dams and embankments. *Geotechnique* 15(2):139–159
- Numada M, Konagai K, Ito H, Johansson J (2010) Material point method for run-out analysis of earthquake-induced long-traveling soil flows. *Env Syst Res* 27:227. <https://doi.org/10.11532/proee2003.27.227>
- Surinach E et al (2005) Seismic detection and characterization of landslides and other mass movements. *Nat Hazards Earth Syst Sci* 5: 791–798
- Tang C-L et al (2012) The mechanism of the 1941 Tsaoling landslide, Taiwan: insight from a 2D discrete element simulation. *Environ Earth Sci* 70(3):1005–1019
- Vilajosana I et al (2008) Rockfall induced seismic signals: case study in Montserrat, Catalonia. *Nat Hazards Earth Syst Sci* 8:805–812
- Wakai A, Cai F, Ugai K, Soda T (2015) Numerical simulation for an earthquake-induced catastrophic landslide considering strain-softening characteristics of sensitive clays. In: Lollino G et al (eds) *Engineering geology for society and territory*, vol 2. Springer, Cham. [https://doi.org/10.1007/978-3-319-09057-3\\_115](https://doi.org/10.1007/978-3-319-09057-3_115)
- Wang R (1999) A simple orthonormalization method for stable and efficient computation of Green's functions. *Bull Seismol Soc Am* 89(3): 733–741 **Accession: 029788774**
- Wang J, Ward SN, Xiao L (2015) Numerical simulation of the December 4, 2007 landslide-generated tsunami in Chehalis Lake, Canada. *Geophys J Int* 201(1):372–376
- Wang YF et al (2018) Normal stress-dependent frictional weakening of large rock avalanche basal facies: implications for the rock avalanche volume effect. *J Geophys Res Solid Earth*. <https://doi.org/10.1002/2018JB015602>
- Wen B et al (2004) Characteristics of rapid giant landslides in China. *Landslides* 1(4):247–261
- Yamada M et al (2013) Dynamic landslide processes revealed by broadband seismic records. *Geophys Res Lett* 40(12):2998–3002
- Yang CM, Chen YR, Dong JJ, Hsu HH, Cheng WB (2015) The normal stress on the slipsurface: a dominating factor on the run-out distance of the sliding rock mass. In: Lollino G et al (eds) *Engineering geology for society and territory*, vol 2. Springer, Cham. [https://doi.org/10.1007/978-3-319-09057-3\\_301](https://doi.org/10.1007/978-3-319-09057-3_301)
- Yang C-M et al (2014) Initiation, movement, and run-out of the giant Tsaoling landslide — what can we learn from a simple rigid block model and a velocity–displacement dependent friction law? *Eng Geol* 182:158–181
- Yuan RM et al (2014) Mechanism of the Donghekou landslide triggered by the 2008 Wenchuan earthquake revealed by discrete element modeling. *Nat Hazards Earth Syst Sci* 14(5):1195–1205
- Zhang Y et al (2015) DDA validation of the mobility of earthquake-induced landslides. *Eng Geol* 194:38–51
- Zou Z et al (2017) Kinetic characteristics of debris flows as exemplified by field investigations and discrete element simulation of the catastrophic Jiweishan rockslide, China. *Geomorphology* 295:1–15